Satellite-observed pollution from Southern Hemisphere biomass burning

David P Edwards, Louisa K Emmons, John C Gille, A. Chu, Jean-Luc Attié, L. Giglio, S.-W. Wood, J. Haywood, Merritt N Deeter, Stevens T Massie, et al.

Satellite-observed pollution from Southern Hemisphere biomass burning

D. P. Edwards,[1] L. K. Emmons,[1] J. C. Gille,[1] A. Chu,[2] J.-L. Attié,[3] L. Giglio,[4] S. W. Wood,[5] J. Haywood,[6] M. N. Deeter,[1] S. T. Massie,[1] D. C. Ziskin,[1] and J. R. Drummond[7]

Received 8 September 2005; revised 14 March 2006; accepted 17 April 2006; published 26 July 2006.

[1] Biomass burning is a major source of pollution in the tropical Southern Hemisphere, and fine mode carbonaceous particles are produced by the same combustion processes that emit carbon monoxide (CO). In this paper we examine these emissions with data from the Terra satellite, CO profiles from the Measurement of Pollution in the Troposphere (MOPITT) instrument, and fine-mode aerosol optical depth (AOD) from the Moderate-Resolution Imaging Spectroradiometer (MODIS). The satellite measurements are used in conjunction with calculations from the MOZART chemical transport model to examine the 2003 Southern Hemisphere burning season with particular emphasis on the months of peak fire activity in September and October. Pollutant emissions follow the occurrence of dry season fires, and the temporal variation and spatial distributions of MOPITT CO and MODIS AOD are similar. We examine the outflow from Africa and South America with emphasis on the impact of these emissions on clean remote regions. We present comparisons of MOPITT observations and ground-based interferometer data from Lauder, New Zealand, which indicate that intercontinental transport of biomass burning pollution from Africa often determines the local air quality. The correlation between enhancements of AOD and CO column for distinct biomass burning plumes is very good with correlation coefficients greater than 0.8. We present a method using MOPITT and MODIS data for estimating the emission ratio of aerosol number density to CO concentration which could prove useful as input to modeling studies. We also investigate decay of plumes from African fires following export into the Indian Ocean and compare the MOPITT and MODIS measurements as a way of estimating the regional aerosol lifetime. Vertical transport of biomass burning emissions is also examined using CO profile information. Low-altitude concentrations are very high close to source regions, but further downwind of the continents, vertical mixing takes place and results in more even CO vertical distributions. In regions of significant convection, particularly in the equatorial Indian Ocean, the CO mixing ratio is greater at higher altitudes, indicating vertical transport of biomass burning emissions to the upper troposphere.

Citation: Edwards, D. P., et al. (2006), Satellite-observed pollution from Southern Hemisphere biomass burning, *J. Geophys. Res.*, *111*, D14312, doi:10.1029/2005JD006655.

1. Introduction

[2] Tropospheric studies have traditionally relied on field campaigns, regular ground-based and aircraft measurements from specific sites, and on an important contribution from chemical-transport modeling. Satellite remote sensing offers the best opportunity of making global measurements of tropospheric trace gases and aerosol over extended periods of time. In this respect it provides an integrating step between observations of emission sources and subsequent in situ measurements taken some distance away, thus allowing the examination of the impact of intense local pollution sources on continental and global-scale air quality. The Terra satellite, launched in December of 1999, now provides 5 years of measurements that allow for a detailed look at pollution events that significantly affect tropospheric air quality. The Measurement of Pollution in the Troposphere (MOPITT) instrument measures carbon monoxide (CO) profiles and the Moderate-Resolution Imaging Spec-

[1]National Center for Atmospheric Research, Boulder, Colorado, USA.
[2]Joint Center for Earth Systems Technology, University of Maryland, Baltimore County, Baltimore, Maryland, USA.
[3]Observatoire Midi-Pyrénées, Toulouse, France.
[4]NASA Goddard Space Flight Center, Greenbelt, Maryland, USA.
[5]National Institute of Water and Atmospheric Research Ltd, Lauder, Central Otago, New Zealand.
[6]Met Office, Exeter, UK.
[7]Department of Physics, University of Toronto, Toronto, Ontario, Canada.

0148-0227/06/2005JD006655

troradiometer (MODIS) derives aerosol optical depth (AOD). Fine mode aerosol particles are produced predominantly as a result of anthropogenic processes. These sources include the burning of fossil fuels in urban and industrial areas, the use of biofuels in developing countries, wildfires, and agricultural burning. These same processes involve incomplete combustion and lead to the emission of CO into the atmosphere. The seasonal and interannual variations of the aerosol AOD and CO Northern Hemisphere (NH) distributions were described in detail by *Edwards et al.* [2004]. Here we concentrate on the CO and AOD signatures of biomass burning in the Southern Hemisphere (SH) to examine in particular the transport of biomass burning products from South America and southern Africa during the August–November peak in the burning season of 2003. Our aim is to investigate the long-range horizontal and vertical transport of these emissions and their impact on the remote atmosphere.

[3] Approximately a half billion hectares of natural and human-induced biomass burning takes place each year. About 85% of this occurs in the tropics for cultivation, deforestation, and savanna grazing. Gas emissions from the fires depend on vegetation type, meteorology, and combustion stage. Most emissions contain carbon, with about 90% emitted as either carbon dioxide (CO_2) or CO, with the remainder in the form of methane (CH_4), nonmethane hydrocarbons (NMHC), and oxygenated volatile organic compounds (O VOC) [*Cautenet et al.*, 1999; *Andreae and Merlet*, 2001]. Carbon monoxide is a very important trace gas in tropospheric chemistry, and its presence in high concentrations affects the oxidizing capacity of the atmosphere [*Logan et al.*, 1981; *Kanakidou and Crutzen*, 1999]. Modeling studies [*Galanter et al.*, 2000; *Intergovernmental Panel on Climate Change*, 2001] suggest that biomass burning is responsible for about 30–40% of the global annual CO budget, and in the tropics it is the most important source of both CO and nitrogen oxide ($NO_x = NO + NO_2$) [*Crutzen and Carmichael*, 1993]. The oxidation of CO and other hydrocarbons in a polluted environment with elevated levels of NO_x, which is produced by fires among other sources, leads to the formation of tropospheric ozone (O_3) [*Ridley et al.*, 1992]. The necessary photochemistry is especially active in the tropical lower troposphere due to abundance of H_2O and the strong solar flux.

[4] Biomass burning also loads the air with carbonaceous particles and mineral ash [*Andreae and Merlet*, 2001]. This contributes to global pollution and potentially impacts weather and climate [*Jacobson*, 2001; *Kaufman et al.*, 2002a]. Aerosols also affect the global budgets of atmospheric oxidants by altering photolysis rates and impact trace gas concentrations by providing sites for heterogeneous chemistry [*Martin et al.*, 2003; *Tie et al.*, 2005]. Depending on the particular fuel, oxygen availability, and combustion phase, smoke from vegetation fires is dominated by fine organic carbon (OC) aerosol with varying amounts of black carbon (BC) [*Andreae and Merlet*, 2001]. The latter is emitted primarily in efficient flaming fires, common in the savanna and cerrado grassland of Africa and South America [*Hao et al.*, 1996], and on average, 12% of African savanna smoke AOD is due to absorption by BC [*Eck et al.*, 2001]. Burning associated with deforestation is common in Amazonia and is associated with lower combustion efficiency, and a larger fraction of the biomass is consumed during the long cool smoldering stage in which OC, rather than BC, is emitted together with large amounts of CO [*Ward et al.*, 1996; *Ferek et al.*, 1998]. The sinks of these aerosols are dry deposition, for both hydrophobic and hydrophilic particles, and wet deposition for hydrophilic particles.

[5] A necessary step toward determining the climatic impact of biomass burning is an analysis of emission sources and their seasonal variations, and of transport, chemistry, lifetime, and resultant pollutant distributions. The influence of biomass burning on regional tropospheric chemistry has been the motivation for several SH field campaigns over the last decade. These include Fire of Savanna (FOS)/Dynamique Et Chimie Atmosphérique en Forêt Equatoriale (DECAFE) in 1991 [*Lacaux et al.*, 1995], Southern African Fire Atmosphere Research Initiative (SAFARI)/Tropical Atmospheric Chemistry Experiment Atlantic (TRACE-A) in 1992 [*Andreae et al.*, 1996], Smoke, Clouds, and Radiation-Brazil (SCAR-B) in Brazil in 1995 [*Kaufman et al.*, 1998], Experiment for Regional Sources and Sinks of Oxidants (EXPRESSO) in 1996 [*Delmas et al.*, 1999], the Pacific Exploratory Mission (PEM-Tropics A) in 1996 [*Hoell et al.*, 1999], and SAFARI-2000 [*Swap et al.*, 2003].

[6] We begin the next section with a brief description of the Terra MOPITT CO and MODIS aerosol and fire-count products. This is followed in section 3 by an examination of the SH meteorology and pollutant distributions that arise from biomass burning during the Austral spring. The continental outflow and long range transport of biomass burning emissions are investigated using a combination of observations and CO "tag" modeling using the MOZART chemical transport model (CTM) [*Horowitz et al.*, 2003]. The export of African emissions over the Indian Ocean is examined in more detail in section 4. Of the 5 years of available Terra data, 2003 represents a fairly "average" year in terms of pollutant loadings from SH biomass burning, and we use this year as a case study when examining monthly variations in section 5. The interannual variability of SH biomass burning is the subject of a forthcoming paper [*Edwards et al.*, 2006]. In section 6 we analyze the correlation between biomass burning emissions of aerosol and CO over South America and Africa and estimate values for the emission ratios of these two pollutants from the satellite observations. This is followed by an investigation of plume decay over the Indian Ocean to derive a value for the aerosol lifetime. Observations and modeling tools are used to study vertical transport of biomass burning emissions in section 7. Conclusions are presented in section 8.

2. Observations From the Terra Satellite

[7] Detecting tropospheric gases from space presents particular problems. A total column retrieval may be possible given a suitable spectroscopic feature, but isolating the tropospheric component is difficult. The MOPITT instrument takes the further step of deriving tropospheric CO profile information by probing the pressure-broadened wings of weak spectral lines with a technique capable of high effective spectral resolution and signal-to-noise. In the case of the MODIS observations, recent developments in

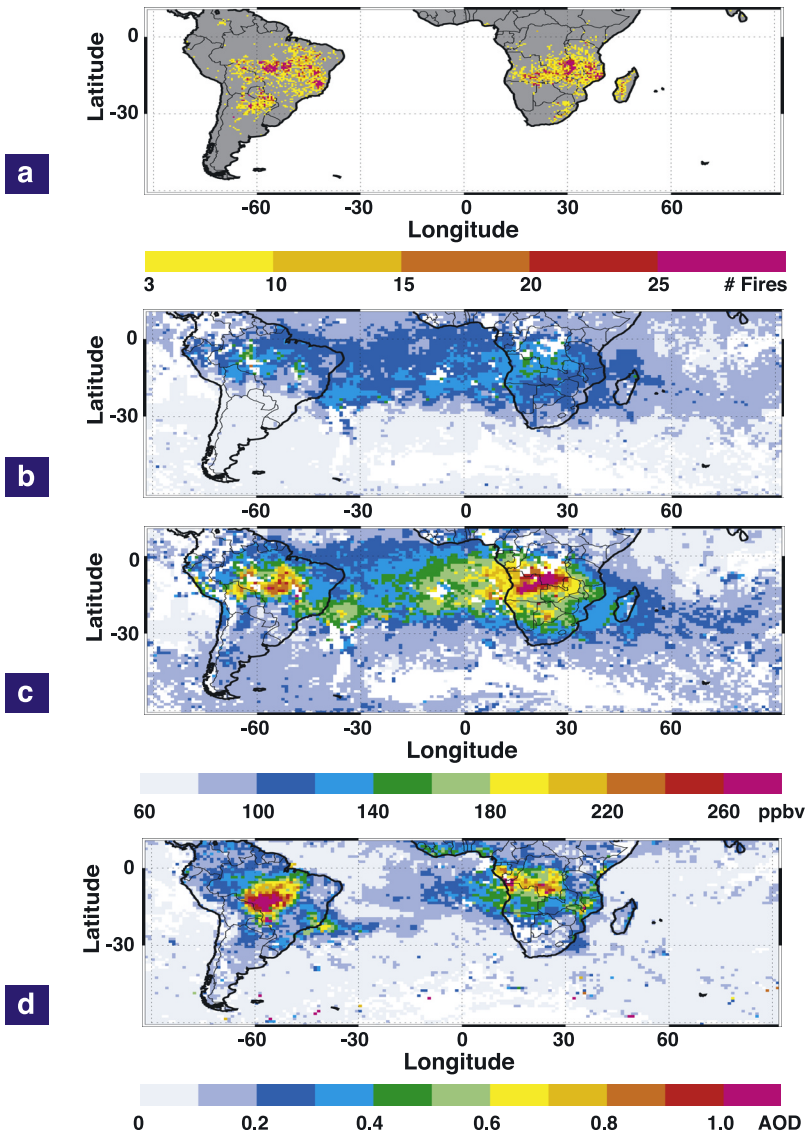

Figure 1. The 23–30 September 2003 mean distributions of (a) MODIS fire counts, MOPITT CO mixing ratio (ppbv) at (b) 250 hPa and (c) 700hPa, and (d) MODIS fine mode AOD.

aerosol retrieval allow the distinction to be made between coarse mode particles and the fine mode particles associated with anthropogenic pollution. Together, the instruments aboard Terra have made significant advances in the remote sensing of tropospheric air quality, and in this paper we make use of 3 different data products from this satellite.

2.1. MOPITT and MODIS Data

[8] Measurements from the joint Canadian-US MOPITT experiment (http://www.eos.ucar.edu/mopitt/) now provide the first, long-term, detailed view of CO emissions in the region. MOPITT is a thermal infrared nadir-viewing gas correlation radiometer, and the instrument, measurement, and retrieval techniques are described in detail by *Drummond* [1992], *Edwards et al.* [1999], and *Deeter et al.* [2003], respectively. We use the daytime retrieved CO mixing ratio profiles and total column from data Version 3 for 2003. The MOPITT retrieval uses a maximum likelihood approach for which the reported mixing ratio at a given level reflects the vertical sensitivity of the measurement as defined by the retrieval averaging kernel and a priori profile [*Rodgers*, 2000; *Deeter et al.*, 2003]. In general, the MOPITT retrieval provides average CO values separately resolved in two relatively broad layers of the atmosphere; in the lower troposphere from about 700 to 500 hPa, and in the upper troposphere from about 300 to 200 hPa [*Deeter et al.*, 2004a; *Kar et al.*, 2004]. Detailed reports on validation exercises are given by *Deeter et al.* [2004b] and *Emmons et al.* [2004].

[9] Southern African biomass burning AOD observations by the multichannel radiometer Terra/MODIS (http://terra.nasa.gov/About/MODIS/about_modis.html) during the SAFARI-2000 field campaign were described by *Ichoku et al.* [2003]. The retrieval of AOD and AOD fraction due to fine mode particles smaller than 0.5 μm at 0.55 μm uses channels in the wavelength range from 0.47 to 2.1 μm which provide spectral information about aerosol optical properties and underlying surface characteristics [*Kaufman*

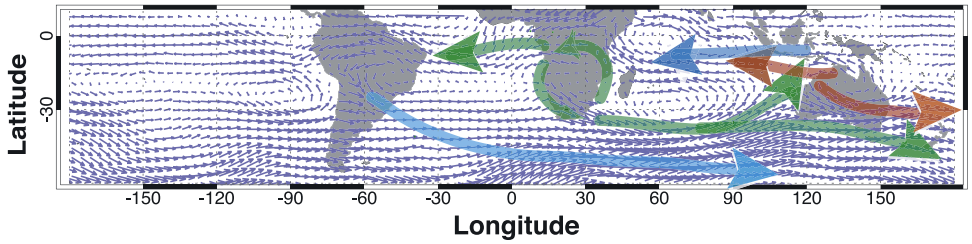

Figure 2. September 2003 mean wind field at the 750 hPa level. Main transport pathways are shown for biomass burning emissions originating in South America, southern Africa, Australia, and Indonesia.

et al., 1997; *Tanré et al.*, 1997; *Remer et al.*, 2002; *Kaufman et al.*, 2002b]. For air quality studies, the AOD and fine mode fraction over land are of particular interest since these particles are primarily of anthropogenic origin [*Chu et al.*, 2002]. In this work we use retrieved AOD and fine-mode fraction from Version 4 which uses assumptions about the aerosol type and size distribution in each geographical region. At the visible wavelengths used, retrievals are not sensitive to aerosol vertical distribution. Validation studies are discussed by *Chu et al.* [2003].

[10] The satellite perspective makes possible the identification of wildfires and biomass burning source regions over large, and often remote, geographical regions. Fire pixels are detected according to absolute and relative difference criteria between various MODIS channels [*Giglio et al.*, 2003]. The $0.5^\circ \times 0.5^\circ$ gridded fire-counts are corrected for spatial variability in the frequency of satellite overpasses and missing observations. To perform such a correction and to reduce the effect of day-to-day variation in fire counts due to cloud obscuration, it is most reliable to generate composite fire count maps for periods of several days. In this paper we use 8-day fire count composites.

3. Southern Hemisphere Biomass Burning Sources and Pollutant Transport

[11] Dry-season biomass burning has a large impact on SH pollutant loadings during the Austral winter and spring [*Edwards et al.*, 2004]. In this section we examine the spatial distribution and seasonal variation of SH biomass burning as indicated by observations from the Terra satellite: MODIS fire counts, the MOPITT CO mixing ratio, and MODIS fine mode AOD. The distributions of these quantities over South America, Africa, and the adjacent oceans for the last week of September 2003 are shown in Figure 1, and a schematic of the main transport pathways is shown in Figure 2 superimposed on the September 2003 mean component wind fields obtained from the National Center for Atmospheric Research/National Centers for Environmental Prediction (NCAR/NCEP) reanalysis in the lower free troposphere at 750 hPa. The degree of correspondence between regions of high fire count and elevated pollution loadings in Figure 1 is variable, both spatially and temporally, and appears to be better over South America than in Africa. Although satellite observations are capable of detecting the presence of a fire and indicate in general terms the location of sources [*Liu et al.*, 2005], care must be exercised when using fire counts alone to infer emissions. Counts do not contain information about the fire intensity, the amount and type of biomass burned, or the specific emissions. This is discussed further in section 5. There are also considerations of measurement sensitivity. AOD is a true column quantity, and high values are often indicative of the higher particulate concentrations in the boundary layer in the vicinity of sources. MOPITT on the other hand is most sensitive to CO plumes in the lower free troposphere that have been vented from the boundary layer, and depending on the prevailing meteorology, this may or may not be close to the emission source. The correlation between MODIS AOD and MOPITT CO is investigated in section 6.

3.1. Africa

[12] In Africa, extensive biomass burning is an annual occurrence. Northern Hemisphere burning in the savanna south of the Sahara Desert and in the tropical rain forests at latitudes just north of the equator takes place from December through April. The location of the burning region moves gradually south with the dry season during the year, although fires are infrequent in the humid Congo Basin area at equatorial latitudes. The transport of CO from these NH regions was previously examined by *Edwards et al.* [2003]. African SH burning starts in about May in the western part of the continent, around Angola and the southern part of the Democratic Republic of the Congo, and later spreads southeast and down the eastern coast. Little burning is observed in the semiarid and arid southwest of the continent. It is estimated that approximately 90% of the biomass burnt in Africa results from savanna fires [*Delmas et al.*, 1999]. The majority of these fires are not wildfires but result from agricultural burning associated with subsistence farming and ranging livestock. By September, fires are widespread across southern Africa and are particularly strong in Angola, the Democratic Republic of the Congo, Zambia, and Mozambique as shown in Figure 1a.

[13] The continent and the adjacent oceans are located in the region of large-scale subsidence occurring between the Hadley and Ferrel cells of the SH general circulation. Figure 2 shows three large anti-cyclonic circulations between 30° S and the equator over the Atlantic Ocean/eastern South America, the African continent, and the Indian Ocean. These are dominant features, particularly in winter, and over the continent they produce spatially ubiquitous and temporally persistent subsidence. This creates stable inversion layers over the burning regions [*Garstang et al.*, 1996; *Swap and Tyson*, 1999] which were observed to persist for up to 40 days during SAFARI-92. In savanna and scrubland, flaming combustion usually dominates in the early burn followed by a later smoldering stage that can

continue for days or even weeks. The stable layers serve as trapping mechanisms for trace gases and aerosols, and emissions are subject to recirculation in the anticyclonic gyre with an associated buildup of pollution. Carbon monoxide mixing ratios of over 300 ppbv at 700 hPa are often observed by MOPITT, along with MODIS fine mode AOD values as high as 2. During SAFARI-2000, the resultant haze layers were observed to extend over thousands of kilometers [*Hobbs*, 2003]. Five frequent transport modes were identified by *Garstang et al.* [1996]: direct easterly or westerly transport, easterly or westerly advection out of an initially anti-cyclonic circulation, and anticyclonic recirculation. These are illustrated in Figure 2. Transport of biomass burning emissions into the Atlantic follows the trade winds and is bounded to the north by the intertropical convergence zone (ITCZ). This plume often travels as far as South America. Measurements taken 2500 km from the African coast at Ascension Island during SAFARI-92 [*Swap et al.*, 1996] and SAFARI-2000 [*Haywood et al.*, 2003] also suggest significant long-range transport of emissions in the lower troposphere and recirculation in the central Atlantic. This provides more time for pollution buildup and photochemical production of O_3. The satellite observations in Figure 1 show persistent high pollution levels in this region. The extensive eastward transport of emissions into the Indian Ocean is discussed in section 5.

3.2. South America

[14] In South America, fires occur annually along the southern edge of the Amazonian rain forest, in the cerrado grasslands and drought-deciduous forest that comprise most of the biomass to the south, and the temperate rain forests along the coast in the east of Brazil [*Fishman et al.*, 1996; *Tansey et al.*, 2004]. In 2003, burning began in June, and by September fires are identified in Brazil, Bolivia, Paraguay, and northern Argentina, Figure 1a. In contrast to the situation in Africa, it was observed during TRACE-A that in Brazil frontal systems generate frequent thunderstorms over burning areas [*Anderson et al.*, 1996]. The resulting deep convection lifts the biomass burning emissions to the free troposphere and leads to higher values and greater variability in both the measured CO and aerosol. On the basis of the study by *Pickering et al.* [1992], 10–40% of CO emitted by biomass fires in a typical burning season over Brazil would be vented out to the free troposphere by deep convection. Topography also plays an important role, and there is significant transport observed along the Andes [*Artaxo et al.*, 1998] before the South American plume exits the continent to the southeast across the Atlantic. At higher tropospheric altitudes, the wind direction is westerly toward Africa, and the combined emissions from Africa and South America result in the Atlantic Ocean become criss-crossed by plumes moving in opposite directions [*Thompson et al.*, 1996; *Chatfield et al.*, 1998].

3.3. Australia and Indonesia

[15] Wildfires in Australia (not shown) occur frequently along the northern and eastern coasts from about September to January, and the fire location determines the transport direction of the resulting biomass burning plumes. MOPITT and MODIS observed emissions from the southeast of the continent are generally taken out over the Pacific Ocean toward New Zealand. Emissions from the north coast are caught up in the Indian Ocean circulation and join some of the emissions from Africa and the emissions from Indonesia to be transported westward into the Indian Ocean just south of the Equator. The fate of pollutants that arrive at this location is discussed further in section 7. Indonesia shows the largest interannual variability in fire season intensity [*van der Werf et al.*, 2003]. Generally, burning takes place during the August–September SH dry season. The dense tropical rainforest in Indonesia, and also in South America, only burns in years when an El Niño warm phase causes significant drying [*Siegert et al.*, 2001]. The second half of 2003 was neutral in terms of the El Niño Southern Oscillation (ENSO) phase as indicated by the Multivariate ENSO Index (MEI) [*Wolter and Timlin*, 1998] and CO and aerosol biomass burning emissions where not high.

3.4. MOZART Calculations

[16] We present results of a study using the MOZART CTM to investigate the CO distribution resulting from SH biomass burning emissions. MOZART was developed at NCAR, the NOAA Geophysical Fluid Dynamics Laboratory at Princeton University, and the Max Planck Institute of Meteorology (Hamburg) to simulate the distribution of tropospheric O_3 and its precursors. A discussion of the model and its evaluation is given by *Horowitz et al.* [2003]. MOZART provides the distribution of 63 chemical constituents, including nonmethane hydrocarbons, between the surface and the upper stratosphere. Here we use the model at a horizontal resolution of about 2.8° in both latitude and longitude (T42). The continuity equations for the simulated species account for advection, convection, diffusive transport, surface emissions, photochemical conversions, and wet and dry deposition. The evolution of species due to all physical and chemical processes is calculated with a time step of 20 min. For this study we use NCAR/NCEP reanalyzed meteorological fields for 2003. Additional tracers (“tags”) are included in this version of the model to represent CO from individual sources and source regions. Biomass burning sources are distributed according to observed fire count data from ATSR [*Arino et al.*, 2001] according to the method described by *Edwards et al.* [2003]. This takes into account the interannual variability in emissions for a given time period. The total CO emissions for the different continental regions were normalized to values from the inventory of G. Pétron et al. (manuscript in preparation, 2005) which is based on the inverse modeling of MOPITT observations for the period 2000–2004 using a method similar to that described by *Pétron et al.* [2004].

[17] The September 2003 700 hPa mixing ratio distributions for CO tags from five SH source regions are shown in Figure 3. The South America region is defined as the area falling between longitudes 90°W and 30°W, latitudes 40°S and the equator; the southern Africa region as 0° to 50°E, 40°S to the equator; the Australia region as 90°E to 160°E, 50°S to 10°S; and the Indonesia region as 90° E to 160°E, 10°S to the equator. For this month, the southern African CO emissions south of 10°S are estimated to be about 17.8 Tg per month. This is similar to the values previously reported for September of 2000, 15.4 Tg per month [*Pétron et al.*, 2004] and 16 Tg per month [*Sinha et al.*, 2004],

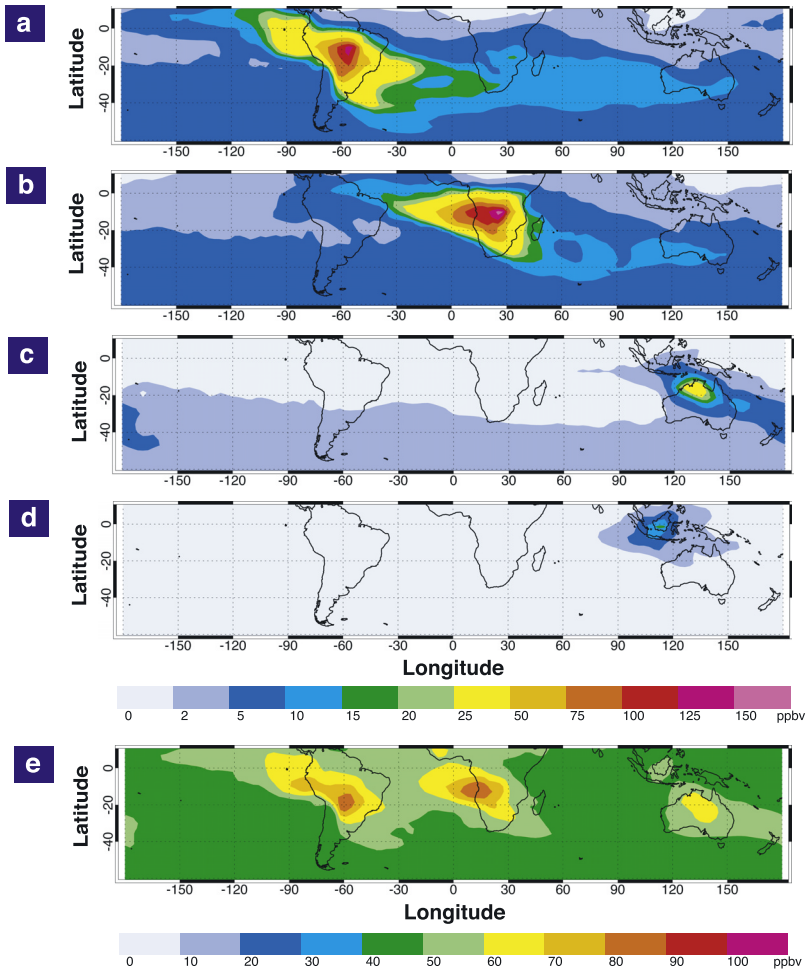

Figure 3. September 2003 average MOZART CO 700 hPa mixing ratio tag plots by source region, (a) South America, (b) Africa, (c) Australia, (d) Indonesia, and (e) CO from chemical production. See text for region definitions.

although we note that in 2000 the peak emission occurred in September, whereas the 2003 emissions rose to a peak of 19 Tg per month in October. The modeled distributions illustrate the main transport pathways. Africa, followed by South America, provided the highest CO loadings. Chemical production of CO, primarily by CH_4 oxidation, provides a uniform background remote from biomass burning source regions [*Granier et al.*, 1999] of about 50 ppbv. Persistent plumes from South America and Africa lead to further enhancements of about 10 ppbv each over the remote oceans. Chemical production from the fast oxidation of hydrocarbons emitted by the fires account for about 70 ppbv or about 30% of the total CO at 700 hPa near sources.

[18] The relative magnitudes of the African emissions exiting to the Atlantic and Indian Oceans depends on the location of the fires and meteorology. For the plumes shown in Figure 3b during September, the CO flux between the surface and 500 hPa crossing imaginary boundaries on the west (11°E), east (42°E), and south (33°S) coasts of southern Africa are 8.9, 4.5, and 9.3 Tg per month, respectively. Since emissions exiting to the south turn eastward into the Indian Ocean almost immediately, this implies that the Indian Ocean receives most of the African biomass burning emissions. This is in general agreement with the previous modeling study of *Sinha et al.* [2004]. Furthermore, MOPITT observations often show plumes exiting Africa over the Atlantic Ocean toward South America that are turned southward on the western edge of the Atlantic/eastern South America anticyclonic circulation and that end up recrossing the Atlantic in an easterly direction at higher southern latitudes. This is particularly frequent during the springtime NH African biomass burning [*Edwards et al.*, 2003] but also occurs with SH biomass burning during the Austral spring. This results in part of the plume originally exiting Africa over the Atlantic finally ending up over the Indian Ocean at high southern latitudes. The Indian Ocean plume is discussed in greater detail in the next section.

4. Indian Ocean Plume in Detail

[19] The dominance of high-pressure patterns over southern Africa varies according to the position of the Walker-Hadley cells and ENSO phase [*Stein et al.*, 2003]. The anticyclonic gyre was not as prevalent during SAFARI-2000 as it had been during SAFARI-92 and reduced the extent of pollution accumulation. This shift away from the dominance of high-pressure patterns increases the frequency

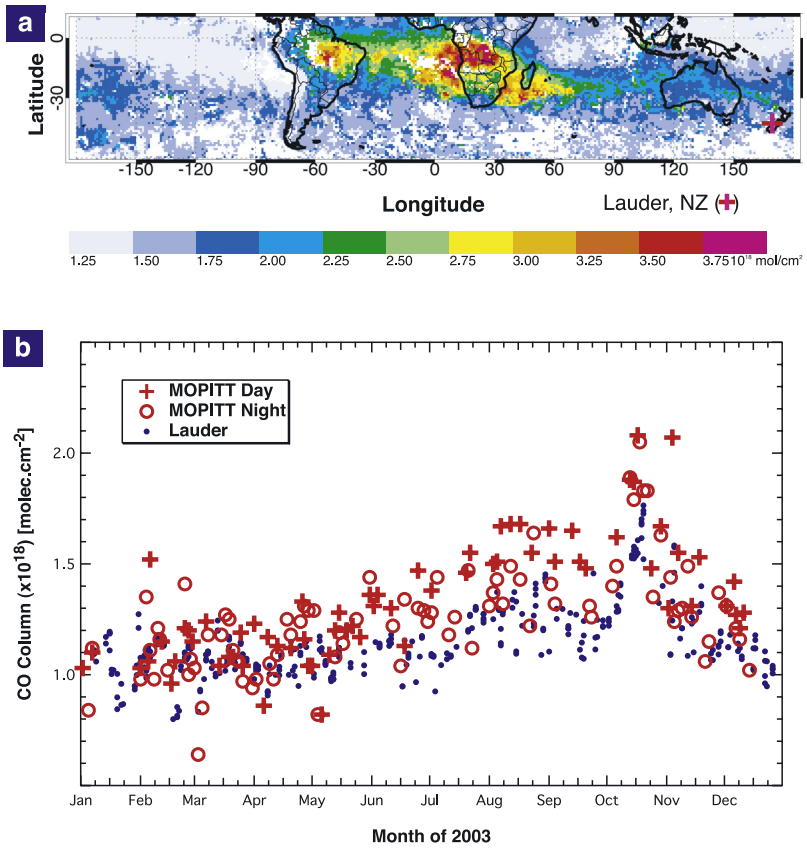

Figure 4. (a) Mean distribution of MOPITT CO total column for 1–9 October 2003, and (b) MOPITT and ground-based FTIR CO total column measurments during 2003 at Lauder, New Zealand.

with which the stable layers are broken by the passage of wave disturbances that allow mixing of pollutants to higher altitudes. This was observed during SAFARI-2000 [*Swap et al.*, 2003] as a "river of smoke" in early September 2000 [*Annegarn et al.*, 2002; *Sinha et al.*, 2004] that produced a pronounced aerosol and trace gas transport corridor off southeastern southern Africa. A similar feature is evident in Figures 1 and 4a (discussed below), and the western edge of the Indian Ocean anticyclonic circulation provides a pathway for funneling biomass burning emissions from southern Africa out into the Indian Ocean, and to higher southern latitudes where the emissions become entrained in the prevailing westerly flow. The aerosol lifetime of a few days in this region is determined primarily by wet deposition, and as a consequence, high AOD levels do not extend far from the source regions. This is discussed further in section 4.1. In contrast, a calculation using MOZART gives a tropospheric chemical lifetime for CO of nearly 2 months at 25°S in September. This is determined primarily by oxidation by the hydroxyl radical (OH). This makes CO an excellent tracer for tropospheric transport processes, and plumes from the strong biomass burning sources are observed extending from Africa across the Indian Ocean toward Australia. During the Austral spring, a band of high CO develops that circumscribes the globe around 30° S with lower troposphere values often reaching twice background CO levels. The regions of highest CO mixing ratio shown in Figures 1b and 1c are in general the same at both the 700 hPa and 250 hPa levels. However, further away from the source regions there are significant differences between the distributions that are discussed in section 7. Part of the Indian Ocean plume continues east over Australia and New Zealand, and part is entrained in the large high-pressure system that is a persistent feature of the SH Indian Ocean during September and October. This delivers biomass burning emissions northward toward Indonesia. In addition to CO and hydrocarbons, biomass burning also produces other ozone precursors. A plume of NO_2, attributed primarily to African biomass burning, is observed by the ERS-2 satellite Global Ozone Monitoring Experiment (GOME) crossing the Indian Ocean during September [*Kunhikrishnan et al.*, 2004]. This is the only time of the year when NO_2 levels reach sufficiently high values that they are observable by satellite in the remote SH ocean. GOME has also observed corresponding elevated tropospheric O_3 levels [*Valks et al.*, 2003], although the distribution also depends on NO_x production by lightning and the effects of long range transport [*Thompson et al.*, 2003; *Fishman et al.*, 2003].

[20] The westerly disturbances which lead to the outflow of biomass burning emissions from southern Africa peak in October [*Garstang et al.*, 1996]. Figure 4a shows the SH distribution of the MOPITT retrieved total CO column for the period 1–9 October 2003. Significant emissions can be seen from South American and southern African biomass burning which produce distinct plumes crossing the Indian Ocean. In addition to this outflow, there are also fire emissions in northern Australia. The effect of these plumes

on the usually clean atmosphere above Lauder, New Zealand, is evident in the Fourier transform interferometer (FTIR) CO total column measurements during this season at the network for the detection of stratospheric change (NDSC) site (45.05° S, 169.68° E), which show a peak in the first half of October. The MOPITT daytime and nighttime CO column measurements are also shown, separately, for pixels falling within a 100 km radius of Lauder with no apparent bias between the two data sets. Generally good agreement in the trends is obtained throughout the year between the MOPITT observations and the interferometer measurements. The FTIR data are not necessarily coincident with the MOPITT daytime measurements, which explains some of the scatter. There is also an apparent positive bias between the MOPITT and the FTIR measurements. This is partly due to the use of a globally invariant a priori profile in the Version 3 MOPITT retrieval which is more appropriate to northern midlatitudes and higher background pollution levels [*Emmons et al.*, 2004], and this produces an overestimation of the column. At the same time, the a priori profile used in the FTIR retrieval is appropriate to relatively clean SH conditions. The instruments also have very different measurement sensitivities. Coincident with SAFARI-2000, *Pak et al.* [2003] made aircraft measurements of air masses arriving in southeast Australia, in the Bass Strait just south of Melbourne. Boundary layer contamination originated from air that had been circulating over Australia and was probably dominated by emissions from Melbourne. Carbon monoxide arriving at 3 and 4 km altitude was traced to biomass burning in southern Africa, with indication that CO at higher altitudes originated in South America. Assuming therefore that the long-range transport of biomass burning emissions takes place in the free troposphere where MOPITT has its maximum vertical sensitivity, it is likely that the column retrieval over Lauder will be high with respect to the FTIR data which are relatively more sensitive to the clean boundary layer. The FTIR measurements also represent local conditions, whereas a larger area must be considered to obtain sufficient MOPITT data for comparison purposes. MOPITT validation work using the NDSC network measurements is currently underway which will explicitly take into account the different instrument averaging kernels and a priori assumptions. Examination of plume propagation in the MOPITT CO and MODIS AOD fields indicates that it takes between 8 and 13 days for pollution to travel between the African and Australian coasts, the longer interval corresponding to plumes that undergo significant southern transport after leaving the African coast. This is at the higher end of the range estimated by the tracer study of *Pak et al.* [2003].

5. Seasonal Variation of Biomass Burning Emissions

[21] Satellite observations of active fires and burn scars has led to greater appreciation of the importance of biomass burning spatial and temporal variability and the effect that this has on emission estimates [*Silva et al.*, 2003; *van der Werf et al.*, 2003]. The SAFARI-2000 campaign provided an opportunity for studies investigating the seasonality of southern African biomass burning emissions in the year 2000. In reviewing the main findings of the campaign, it was noted by *Swap et al.* [2003] that there existed an apparent anomaly between different estimates of when the seasonal peak in fire activity and emissions occurred. Satellite observations indicated a maximum in fire-scar burned area in June and July [*Silva et al.*, 2003], in agreement with subsequent estimates of the peak month for CO emissions based on a "bottom-up" approach combining burn-scar data with models providing available biomass loading and combustion parameters [*Hoelzemann et al.*, 2004]. However, surface Sun photometer AOD measurements [*Queface et al.*, 2003] in Mozambique indicated strong increases in aerosol loading from August to October, and the same seasonality was also observed in AERONET measurements [*Eck et al.*, 2003]. It has been argued [*Stein et al.*, 2003; *Swap et al.*, 2003] that the later seasonality coincides with the peak frequency of synoptic conditions favoring eastward transport of pollution over the measurement sites, rather than a later peak in the actual emissions.

[22] To examine these questions from the larger satellite perspective, we discuss the seasonality of the pollutant loadings over each of the SH regions defined in section 3.4. Figure 5 shows the 2003 seasonal variation of MODIS fire counts, MOPITT 700 hPa CO mixing ratio, and MODIS fine mode AOD. In southern Africa, the maximum number of fire counts were observed in late August. However, the pollution emitted by these fires, as indicated by the CO loading at 700 hPa and the fine mode AOD, peaks later in September and October when the fire count, although still high, is decreasing. This is consistent with the seasonality of the emissions inventory of *Pétron et al.* [2004] using a "top-down" inversion of the MOPITT data. The fact that the CO and AOD time series follow each other well and show peaks at about the same times suggests that this is not because of delayed detection due to issues related to the different measurement vertical sensitivities of the two instruments. A similar seasonality is observed in the CO and AOD loadings in 2000 (not shown), suggesting that the seasonality of the local aerosol measurements during SAFARI-2000 was indeed representative of the continental scale.

[23] It is still unclear why there is a time lag between the peaks in fire counts and pollutant loadings over southern Africa. Local meteorological controls may play a role in determining vertical mixing and the trapping of pollutants that changes with the transition from Austral winter to spring. To examine this further, we used MOZART to separately tag the CO emissions for each week from August to October. This allowed an estimate of the CO residence time over the continent between emission and export. Results indicated that 75% of the CO would be exported in about 8 days, a much shorter time than the observed time lag of nearly a month. Another possible explanation currently being examined in "bottom-up" model emissions studies (G. R. van der Werf, private communication, 2005) is that denser wooded vegetation burns at the end of the fire season in small fires that are either not detected or that produce relatively higher emissions per fire. It may also be that the long smoldering fire phase would produce high emissions for sometime after the peak in satellite detection of flaming fires.

[24] Over South America, there is good correspondence in the timing of peaks in fire-count, CO, and AOD. A

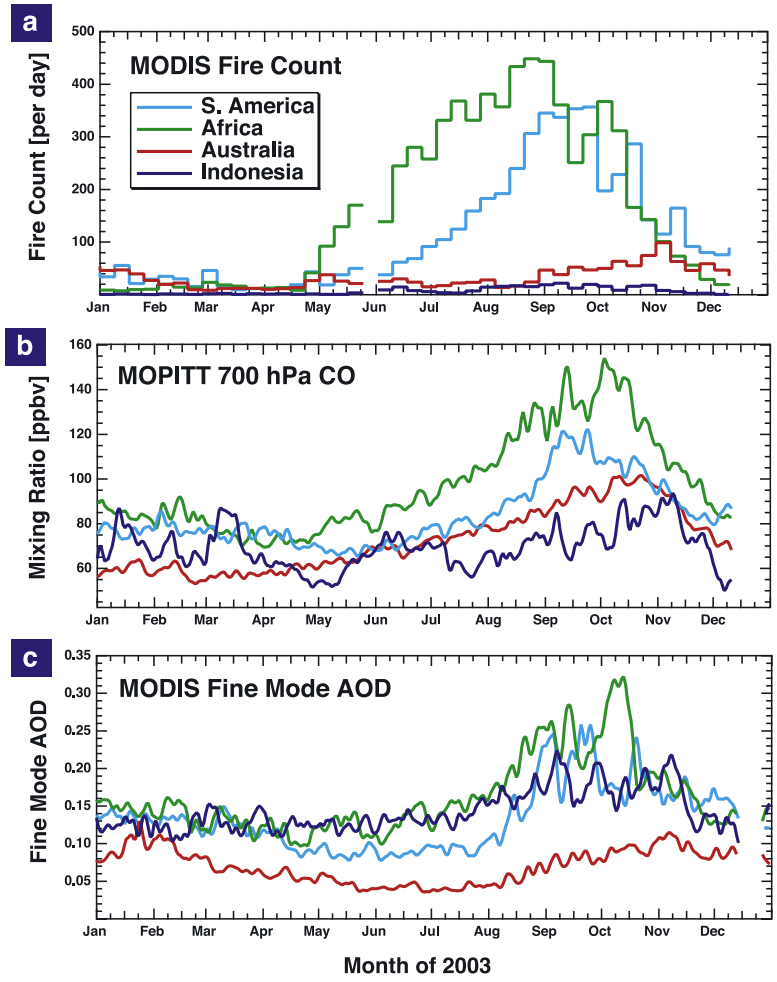

Figure 5. Year 2003 seasonal variation in (a) MODIS fire-count, (b) MOPITT CO 700 hPa mixing ratio (ppbv), and (c) MODIS fine mode AOD. See text for region definitions.

maximum is reached in September and October, and the pollutant loadings over the region are relatively low before this time. This seasonality is in general agreement with other studies [*van der Werf et al.*, 2003]. As noted previously, CO that is observed over South America earlier in the year before the onset of local burning is often due to transported emissions from fires in south equatorial Africa. The fire-count observations in Australia reached a maximum in November. This was a time of widespread fires across the Kimberly Plateau in northern Australia. It can be seen from Figure 5 that there is reasonable agreement between the timing of the fires and the AOD loading over this region. The CO loading, however, has a maximum in October, before the peak in the fires. This is due to the contribution of transported CO from African biomass burning rather than the result of local emissions. During 2003, the fire density in Indonesia was low, and the peak burning occurred from August to November. However, relative to the MOPITT CO, the MODIS AOD is particularly large when compared to the ratio of the two pollutants over other regions. In an analysis of MODIS retrievals during SAFARI-2000 [*Ichoku et al.*, 2003; *Schmid et al.*, 2003], it was found that a single value of the single scattering albedo is inadequate for global smoke aerosol retrieval, and that the employed value should better represent the particular particles considered. The overestimation of the AOD over Indonesia is most probably the result of an assumed single scattering albedo that is too low [*Gras et al.*, 1999].

6. Correlation Between CO and AOD

[25] The locations of high values of MOPITT CO mixing ratio and MODIS AOD shown in Figure 1 show fairly good correlation. This is expected because direct emissions of CO and carbonaceous aerosol from common sources dominate the local fields [*Edwards et al.*, 2004]. This can be contrasted to the poor correlation often obtained over urban regions where the principal aerosol contributing to the regional fine mode AOD is often sulfate arising from industrial SO_2 emissions. In general, we find that over areas of biomass burning, the pollutant correlation is highest for the first few days at the start of new burning when the individual plumes of CO and aerosol are distinct. The correlation may not be as good at later times when the CO field is not representative of recent local emissions because of the significantly longer CO lifetime and the fact that "older" CO from earlier fires also contributes to the column. The degree of correlation also depends on the

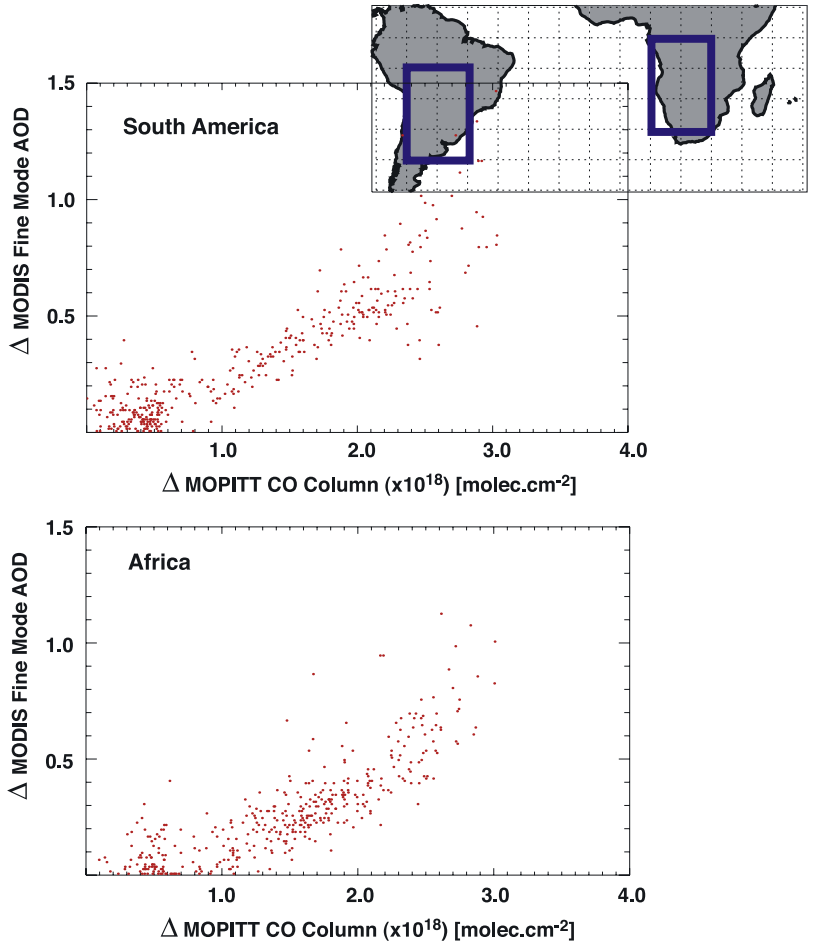

Figure 6. Scatter plot of MODIS fine mode AOD and MOPITT CO total column perturbations above background over regions of South America (40°S–10°S, 70°W–50°W), and Africa (30°S–0°, 10°E–30°E), for 4–8 September 2003.

different vertical sensitivities of the two measurements. Observations of CO allow for fairly accurate estimation of other fire emissions that cannot be measured directly because of the close correlations that often exist between CO and other trace gases emitted during smoldering combustion [*Andreae and Merlet*, 2001].

6.1. An Estimate of the Aerosol/CO Emission Ratio

[26] Examples of the correlation between biomass burning enhancements in MODIS fine mode AOD and MOPITT CO column are shown in Figure 6 where the daily 1° gridded values are compared separately for regions in South America (40°S–10°S, 70°W–50°W) and Africa (30°S–0°, 10° E–40°E) during 4–8 September 2003. The gradient of a fit to these scatter distributions, which we denote by G, can be expressed as

$$G\left[\text{molec}^{-1}.\text{cm}^2\right] = \frac{AOD_P - AOD_{BG}}{CO_{col,P}\left[\text{molec.cm}^{-2}\right] - CO_{col,BG}\left[\text{molec.cm}^{-2}\right]} \quad (1)$$

and distinguishes between plume (P) and background (BG) concentrations. In order to represent the enhancement of AOD normalized to the enhancement of CO column as a reference, background values of 0.0141 and 1.11×10^{18} molec.cm^{-2} have been subtracted from the MODIS AOD and MOPITT CO column retrievals, respectively. These values are representative of the remote SH ocean. In both cases, the correlation between the measurements is very good. For the South American region, the values of the correlation coefficient and G are 0.89 and $3.06 \pm 0.08 \times 10^{-19}$ molec^{-1}.cm^2, respectively. For the African region, these values are 0.83 and $2.53 \pm 0.08 \times 10^{-19}$ molec^{-1}.cm^2. The quantity G can be used to estimate the aerosol emission ratio ER with respect to CO. Since the measurements are of column quantities, for which we have limited information on CO vertical distribution and no profile information for aerosol, we make the assumption that these column measures are dominated by a particular layer in the lower troposphere. This is often the case as observed by *Anderson et al.* [1996] during TRACE-A, and in addition, biomass burning CO and aerosol often show similar vertical distributions. During SAFARI-2000, *Haywood et al.* [2003] observed that profiles of aerosol number density and CO concentration were well correlated within regional haze resulting from extensive burning. If the dominant layer is characterized by an altitude depth Δz, pressure depth Δp,

and has mean pressure and temperature values $\bar{p}$ and $\bar{T}$, respectively, then the average CO mixing ratio CO_q is related to the total column CO_{col} by

$$CO_q = \frac{M_r g}{\Delta p}\, CO_{col}, \tag{2}$$

where g is the acceleration due to gravity and we are assuming an ideal gas of molecular weight M_r and static equilibrium. The average aerosol mass density within the layer is

$$\rho = \frac{AOD}{k_e}\,\frac{1}{\Delta z}, \tag{3}$$

where k_e (at 0.55 μm) is the specific extinction coefficient. After noting that

$$\frac{\Delta p}{\Delta z} = \frac{M_r g \bar{p}}{R\bar{T}}, \tag{4}$$

where R is the gas constant per mole, the ratio of the layer average aerosol mass density to CO mixing ratio can be written

$$\frac{\rho}{CO_q} = \frac{AOD}{CO_{col}}\,\frac{\bar{p}}{R\bar{T}}\,\frac{1}{k_e}. \tag{5}$$

Assuming the aerosol material density m and the single particle volume V are known, the aerosol mass density ρ can be substituted by NVm where N is the aerosol number density. This leads to

$$\frac{N}{CO_q} = \frac{AOD}{CO_{col}}\,\frac{\bar{p}}{R\bar{T}}\,\frac{1}{k_e V m}. \tag{6}$$

In commonly used units, the aerosol number density emission ratio with respect to CO concentration can then be written as

$$\begin{aligned} ER\left[\mathrm{cm^{-3}.ppbv^{-1}}\right] &= \frac{N_P[\mathrm{cm^{-3}}] - N_{BG}[\mathrm{cm^{-3}}]}{CO_{q,P}[\mathrm{ppbv}] - CO_{q,BG}[\mathrm{ppbv}]} \\ &= 0.724 \times G\left[\mathrm{molec^{-1}.cm^2}\right] \\ &\quad .\frac{\bar{p}[\mathrm{hPa}]}{\bar{T}[\mathrm{K}]}\,\frac{1}{k_e[\mathrm{m^2.g^{-1}}]\; m[\mathrm{g.cm^{-3}}]\; V[\mathrm{m^3}]} \end{aligned} \tag{7}$$

For the aerosol parameters, we use mean values measured during SAFARI-2000 aircraft flights [*Haywood et al.*, 2003, Table 2]. For single particle volume, V = 8.0 ± 1.9 × 10^{-21} m^3, and for specific extinction, k_e = 4.3 ± 0.5 $m^2.g^{-1}$. In deriving particle volumes, three lognormal size distributions were used. Particle density m for biomass burning smoke is taken as 1.35 ± 0.15 $g.cm^{-3}$ [*Reid et al.*, 1998]. In the absence of correspondingly detailed particle size distribution data for South America, we use the SAFARI aerosol parameter values for both the African and South American regions. For an estimate of $\bar{p}/\bar{T}$ for the contributing atmospheric layer, MOZART was used to average this ratio for grid points falling within the regions of interest between the surface and 700 hPa. This yielded values of 2.96 ± 0.32 $hPa.K^{-1}$ and 2.90 ± 0.25 $hPa.K^{-1}$ for South America and Africa, respectively. Estimates of the aerosol number density emission ratio with respect to CO concentration, *ER*, are then 14.2 ± 4.4 $cm^{-3}.ppbv^{-1}$ for the South American region and 11.5 ± 3.5 $cm^{-3}.ppbv^{-1}$ for the African region.

[27] These values are not significantly different, in agreement with the findings of *Anderson et al.* [1996] from TRACE-A measurements. They also fall within the range of previously reported values for these quantities from aircraft in situ measurements during field campaigns. *Anderson et al.* [1996] obtained values for Brazilian and African source regions of 22.5 ± 9.7 $cm^{-3}.ppbv^{-1}$ and 23.6 ± 15.1 $cm^{-3}.ppbv^{-1}$, respectively. For aged biomass plumes over the south Atlantic, *Andreae et al.* [1994] obtained a value of 5.2 ± 1.7 $cm^{-3}.ppbv^{-1}$. During SAFARI-2000, *Formenti et al.* [2003] measured *ER* for aged biomass burning plumes in the range 4–19 $cm^{-3}.ppbv^{-1}$, and for young plumes in the range 26–30 $cm^{-3}.ppbv^{-1}$. These campaign values of ER are higher for young plumes than for aged plumes, and our values appear more representative of aged plumes over the continent. This is probably not surprising given that the satellite total column optical properties are representative of relatively large spatial scales, and would be less sensitive to the fine scale structure of young plumes. This suggests that the satellite derived *ER* would provide a good representative value at the several degree horizontal scales of global CTMs, and the technique could prove useful as input to modeling studies concerned with fires in remote regions in the absence of field data.

6.2. An Estimate of Biomass Burning Aerosol Lifetime

[28] Owing to the longer CO lifetime, there is a sharper decline in the value of fine mode AOD compared to CO concentration in plumes as they exit the continents (Figure 1). The CO lifetime depends primarily on oxidation by OH and this is well represented by chemical-transport models such as MOZART. It is certainly better quantified than the aerosol lifetime which is determined over the ocean primarily by wet deposition processes. Plume AOD and CO concentration will both decrease with distance traveled due to dilution. However, the ratio of these quantities should be independent of dilution, and the coincident measurements of both pollution plumes offer a way to estimate the regional aerosol lifetime.

[29] We examine this for the case of the strong plumes exiting the east coast of Africa over the Indian Ocean in the first week of October, 2003. The CO column distribution for this time period is shown in Figure 4. With the exception of southerly transport off the coast of South Africa for some plumes at the beginning of their trajectories, transport is almost due east toward Australia, and the ratio G can be mapped as a function of longitude to indicate its time evolution assuming that the CO plumes are of about the same age when they leave the African coast. As shown by (7), G is proportional to the ratio of the aerosol and CO number densities. The plume decay is illustrated in Figure 7 where the values of G have been calculated for all daily 1° × 1° gridded values falling within 2° wide longitude bins

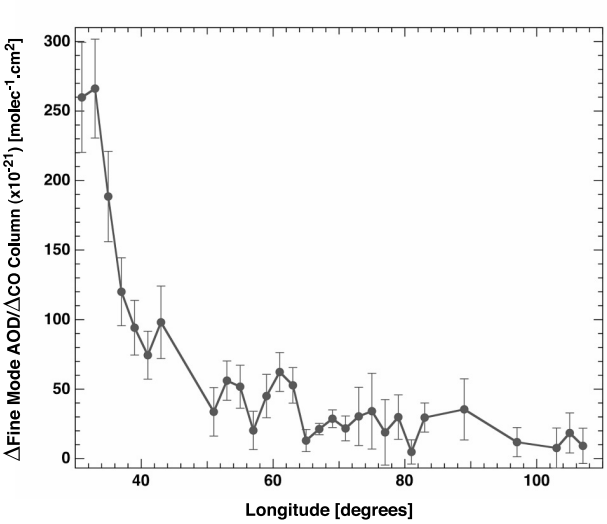

Figure 7. Longitudinal variation of the ratio of enhanced MODIS fine mode AOD to MOPITT CO column for biomass burning plumes exiting southern Africa over the Indian Ocean. Observations in the latitude band 40°S–15°S for the period 1–9 October 2003.

between the latitudes 40°S and 15°S over the time period 1–9 October 2003. Only ocean pixels are used. This includes multiple plumes that leave the African coast at different times with the passage of wave disturbances as described in section 4. We assume that the aerosol number density and CO concentration individually decay exponentially with time t [*Brasseur et al.*, 1999] such that

$$G(t) = G(0)\frac{\exp(-t/\tau_{aero})}{\exp(-t/\tau_{CO})}, \tag{8}$$

where τ_{aero} and τ_{CO} are the aerosol and CO lifetimes. This leads to

$$\ln G(t) = \ln G(0) - t\left(\frac{1}{\tau_{aero}} - \frac{1}{\tau_{CO}}\right). \tag{9}$$

From MOZART, τ_{CO} for this time period and latitude range is about 61 days. An estimate of τ_{aero} can be obtained from the gradient of the log of the data shown in Figure 7 after making the transformation

$$t[\text{days}] = \frac{Longitude(t) - Longitude(0)}{v\left[\text{deg.day}^{-1}\right]}, \tag{10}$$

where v is the observed plume velocity in degrees of longitude per day. This is estimated as 8 ± 2 deg.day^{-1} from tracing specific plumes, which are especially clear in the MODIS AOD data. The lower plume velocity corresponds to locations close to Africa where there is often an initial trajectory to the southeast, whereas further into the Indian Ocean the plumes make faster progress to the east. A value for the aerosol lifetime τ_{aero} can then be calculated, and we obtain 3.8 ± 0.8 days for this quantity.

[30] Biomass burning aerosol optical properties change during plume aging through coagulation and by becoming more hygroscopic [*Formenti et al.*, 2003; *Reid et al.*, 2005]. The assumed ambient size distributions used in the MODIS AOD retrieval are based on AERONET measurements from land-based sites. For aerosol retrieval over ocean, there is limited information from the small number of island sites. Aging is likely to increase the single-scattering albedo [*Abel et al.*, 2003]. Over land, the MODIS retrieval assumes a single value of this parameter by region, and over ocean it can vary depending on the selected aerosol model, although this does not change significantly for a given plume. There is therefore the potential for an underestimation of the plume AOD far from the source compared to its retrieved

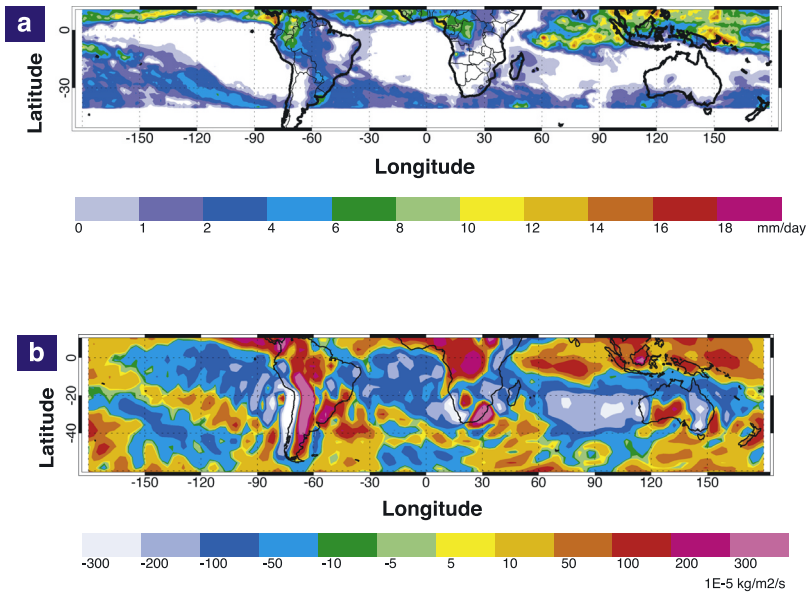

Figure 8. Average September 2003 distributions of (a) TRMM merged precipitation product, and (b) MOZART CO net vertical flux (advection and convection) through the 500 hPa level.

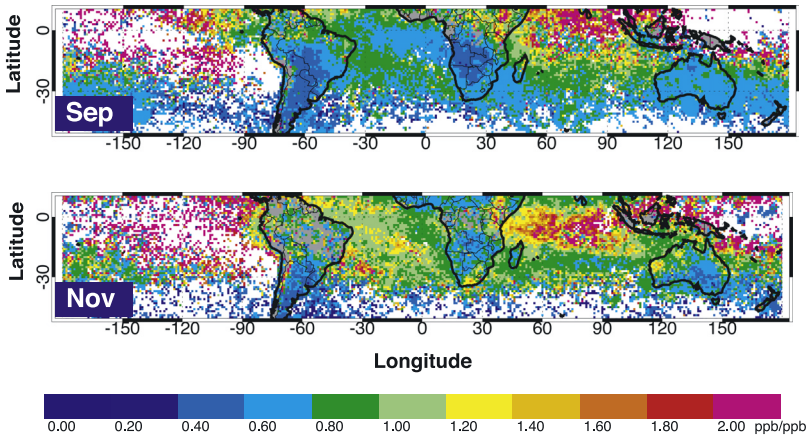

Figure 9. Mean monthly ratios of MOPITT CO mixing ratio retrievals between 250 hPA and 700 hPa for September and November, 2003. No data are shown for cloudy pixels or for background conditions where the CO mixing ratio is less than 100 ppbv at both levels.

value close to the source, although this effect has not been quantified. This suggests that our estimate of τ_{aero} may be on the low side, although it is not too different from global model estimates that put carbon aerosol lifetime at less than about 5 days [*Rasch et al.*, 2000; *Chin et al.*, 2002].

7. Vertical Transport of Emissions

[31] Over tropical continents, convection exports large amounts of pollution from biomass burning [*Fishman et al.*, 1991], and in addition to examining the long-range transport of biomass burning plumes, the vertical transport may also be investigated using CO profile information. Figure 8a shows the average Tropical Rainfall Measuring Mission (TRMM) merged precipitation map for September 2003. The presence of high precipitation may be used as an indication for significant convective activity [*Sobel et al.*, 2004], and this is frequent in equatorial regions at the ITCZ. Examination of the TRMM data show that large and persistent areas of precipitation are present over Indonesia and the southern equatorial Indian Ocean from 60°E–90°E from September 2003 through to February 2004. Further evidence of the strong convection in these areas is provided by the corresponding outgoing longwave radiation (OLR) distributions (not shown) where low values of OLR indicate high cloud tops. This upwelling is associated with the typical Walker circulation, as characterized by neutral monthly values of the MEI for second half of 1993. The MOZART model can also be used to indicate CO net vertical flux resulting from convection and large-scale advection. This is shown in Figure 8b for total CO at the 500 hPa level for September, 2003. Areas of high upward CO flux correspond well in general to high precipitation in the TRMM distribution. The Atlantic Ocean close to Africa and the main pathway for export of biomass burning emissions across the Indian Ocean at about 30°S are not areas of strong uplift.

[32] A convenient way to illustrate the variation in vertical CO distribution is to compare the MOPITT CO retrievals at 250 hPa and 700 hPa, shown in Figure 1, by taking the ratio of the mixing ratios on a pixel-by-pixel basis. Figure 9 shows the monthly means of this ratio for September and November of 2003. No data are shown for cloudy pixels or for background CO conditions where the mixing ratio is less than 100 ppbv at both levels. Only daytime measurements are used here to maximize the information content with respect to the vertical CO distribution. Examination of the retrieval degrees of freedom of signal (DFS) [*Deeter et al.*, 2004a] for this month (not shown) indicates that there is significant vertical profile information (DFS > 1.5) in the MOPITT signals northward of about 45°S.

[33] We consider first the distribution for September. Close to the continental source regions Figure 9a indicates much higher CO concentrations at the lower altitude relative to the higher altitude. These extend along the previously defined export pathways. This is the case even when there are elevated CO concentrations at 250 hPa, as shown Figure 1b, and strong vertical transport, as indicated in Figure 8b. At progressively greater distances from the biomass burning sources, the ratio indicates relatively greater concentrations of CO at the higher altitude. The CO ratio close to unity in the Atlantic is due to CO originating in Africa that is convected as the main plume circulates to the area of uplift indicated in Figure 8 outside of the Atlantic anticyclonic system. Further south, at about 30°S, the profile is again weighted toward the lower level as it becomes dominated by South American outflow close to the source regions. Over the Indian Ocean, the lower free troposphere transport pathway from southern Africa toward Australia and continuing over the Pacific Ocean is clearly defined. This is in contrast to the southern equatorial Indian Ocean where the CO concentration in the upper troposphere approaches twice that at the lower 700 hPa level. As indicated in Figure 8, this is an area of persistent strong convection associated with the ITCZ. In the SH, biomass burning emissions arrive in this area from Indonesia, Australia, and eventually from Africa. There is probably also a component of this pollution that comes from sources in India and southeast Asia, although the ITCZ remains an effective barrier to interhemispheric transport of Asian emissions [*de Laat et al.*, 2001]. Even though pollutant outflow may be distributed vertically throughout the troposphere, the strong uplift concentrates the emissions at the

higher altitudes. We also see an indication of persistent high aerosol extinction in this location during the Austral spring in occultation data from the Stratospheric Aerosol and Gas Experiment (SAGE) [*Kent et al.*, 1998] at upper tropospheric tangent heights. The future availability of higher vertical resolution CO profile measurements from the Aura platform should make it possible to determine to what extent this mechanism constitutes a significant pathway for the injection of biomass burning pollutants into the lower stratosphere.

[34] By November, the SH biomass burning season is coming to an end. Without a continued input of low-altitude CO from the source regions, the aged CO is gradually distributed vertically throughout the troposphere. In regions of significant convection, as indicated by Figure 8b, this leads to a concentration of CO in the upper troposphere.

8. Conclusions

[35] The combination of measurements from tropospheric satellite sensors will play an increasingly important role in explaining chemistry and transport processes in the lower atmosphere. In this study, we have used MOPITT CO concentration and MODIS fine mode AOD measurements in conjunction with calculations from the MOZART CTM to examine the distributions, transport, and seasonal variability of CO and aerosol in SH biomass burning plumes during 2003. The main conclusions of this work may be summarized as follows:

[36] 1. Pollutant emissions follow the occurrence of dry season fires, and the temporal and spatial distributions of MODIS fire counts, MOPITT CO, and MODIS AOD are generally similar. SH transport is governed to a large extent by the three anticyclonic circulations over the Atlantic Ocean, African continent, and the Indian Ocean that are dominant features in the Austral spring. Over Africa and the south Atlantic especially, these high-pressure systems serve as trapping mechanisms for trace gases and aerosol leading to an observed buildup of pollution. Close to sources, CO mixing ratios of over 300 ppbv at 700 hPa are often observed by MOPITT, along with MODIS fine mode AOD values as high as 2. The satellite observations indicate that the transport of African biomass burning emissions follow the five modes identified by *Garstang et al.* [1996]. Emissions from South America exit the continent to the southeast across the Atlantic, which become crisscrossed by plumes moving in opposite directions.

[37] 2. Most of the African emissions find their way into the Indian Ocean. Particularly strong plumes are observed in October 2003, reaching Australia in 8–13 days, where they are further enhanced by local fire emissions before continuing on over the Pacific Ocean. The nearly 2-month lifetime of CO at these latitudes make it an excellent tracer of tropospheric transport, and CO plumes circumscribe the globe with lower troposphere values often reaching twice the background levels of about 50 ppbv. We have demonstrated the impact of African biomass burning on the usually clean atmosphere over New Zealand using both MOPITT and local ground-based FTIR measurements. These observations agree in both the magnitude and seasonality of the pollution enhancement which peaks in October.

[38] 3. Of the SH biomass regions in South America, southern Africa, Australia, and Indonesia, Africa followed by South America contribute most to the zonal pollutant loading. In general, there is good correspondence between the timing of peaks in fire counts, CO concentration and AOD over each of the source regions. However, there are notable exceptions. Over Africa, there is an apparent lag between the peak fire count in late August and peak pollutant loadings in early October. A similar anomaly was observed in data from the SAFARI-2000 campaign. An experiment with MOZART suggests that this is not due to extensive entrapment of pollutants in the continental gyre, and this remains an open issue. Over Australia, peak CO loading is observed in October, about a month earlier than the fire count peak. This is due to pollution export from African fires.

[39] 4. The correlation between enhancements of AOD and CO column for distinct biomass burning plumes is very good with correlation coefficients greater than 0.8 for South American and African examples. This is expected because direct emissions of CO and carbonaceous aerosol from common sources dominate the local fields. A method using MOPITT and MODIS data for estimating the aerosol number density to CO concentration emission ratio has been presented, and yields values of 14.2 ± 4.4 cm^{-3}.ppbv^{-1} and 11.5 ± 3.5 cm^{-3}.ppbv^{-1} for the South American and African regions, respectively. These values are not significantly different and are in general agreement with previous aircraft in situ measurements during field campaigns. These latter measurements also suggest that the satellite derived emission ratios are representative of aged plumes at relatively large spatial scales. This technique could prove useful as input to modeling studies in remote regions in the absence of field data. We have also investigated plume decay after export into the Indian Ocean of emissions from African fires. Together with a MOZART calculation of the CO lifetime, which is relatively well quantified and depends primarily on OH oxidation, examination of the ratio of AOD compared to CO column plume enhancement provides an estimate of the regional aerosol lifetime which is due primarily to wet deposition. We obtain a value of 3.8 ± 0.8 days for this quantity.

[40] 5. Vertical transport has been investigated using CO profile information. Close to source regions, the MOPITT retrieval of CO mixing ratio at 700 hPa is 3 to 4 times that at the 250 hPa retrieval level. Downwind of the continents, vertical mixing takes place and by the time African emissions have reached the mid-Atlantic, the vertical CO mixing ratio profile is close to constant, at about 110 ppbv. Regions of significant convection, as indicated by TRMM precipitation maps, correspond well with MOZART calculations of high CO upward flux. These regions are particularly noticeable near the ITCZ, especially in the Indian Ocean south of the equator and over Indonesia. Here the MOPITT observations indicate that the 250 hPa CO mixing ratio is twice that at 700 hPa. Since this CO originated in biomass burning over Indonesia, Australia, and to a lesser extent, Africa, these measurements suggest a mechanism for the vertical transport of pollutants to the upper troposphere.

[41] This 2003 case study shows that biomass burning emissions under the influence of the prevailing meteorology provide for both low altitude intercontinental transport of pollution together with a mechanism for delivering emission products to the upper troposphere. This is important for

quantifying the effect of local emissions on the larger-scale pollution distribution and also for providing a regional or global context for measurements taken at a specific time and location.

[42] **Acknowledgments.** We wish to thank the MOPITT team at NCAR, Boulder, Colorado, USA, for data processing and algorithm support. MOPITT instrument operations were supported by the MOPITT team at the University of Toronto, Toronto, Ontario, Canada. NCEP Reanalysis data were provided by the NOAA-CIRES Climate Diagnostics Center, Boulder, Colorado, USA, from their Web site at http://www.cdc.noaa.gov/. We thank one of the anonymous reviewers for insights into the role of meteorology in determining vertical mixing of biomass burning emissions. DPE acknowledges NASA support under grant NNG04GA45G and JRD acknowledges the support of the Canadian Space Agency. The National Center for Atmospheric Research is sponsored by the National Science Foundation.

References

Abel, S., J. M. Haywood, E. J. Highwood, J. Li, and P. R. Buseck (2003), Evolution of biomass burning aerosol properties from an agricultural fire in south Africa, *Geophys. Res. Lett.*, *30*(15), 1783, doi:10.1029/2003GL017342.

Anderson, B. E., W. B. Grant, G. L. Gregory, E. V. Browell, J. E. Collins, G. W. Sachse, D. R. Bagwell, C. H. Hudgins, D. R. Blake, and N. J. Blake (1996), Aerosols from biomass burning over the tropical South Atlantic regio: Distributions and impacts, *J. Geophys. Res.*, *101*, 24,117–24,137.

Andreae, M. O., and P. Merlet (2001), Emission of trace gases and aerosols from biomass burning, *Global Biogeochem. Cycles*, *15*(4), 955–966.

Andreae, M. O., B. E. Anderson, D. R. Blake, J. D. Bradshaw, J. E. Collins, G. L. Gregory, G. W. Sachse, and M. C. Shipham (1994), Influence of plumes from biomass burning on atmospheric chemistry over the equatorial and tropical South Atlantic during CITE 3, *J. Geophys. Res.*, *99*, 12,793–12,808.

Andreae, M. O., J. Fishman, and J. Lindesay (1996), The Southern Tropical Atlantic Region Experiment (STARE): Transport and Atmospheric Chemistry near the Equator–Atlantic (TRACE A) and Southern African Fire-Atmosphere Research Initiative (SAFARI): An introduction, *J. Geophys. Res.*, *101*, 23,519–23,522.

Annegarn, H. J., L. Otter, R. J. Swap, and R. J. Scholes (2002), Southern Africas ecosystem in a test-tube: A perspective on the Southern African Regional Science Initiative (SAFARI 2000), *S. Afr. J. Sci.*, *98*, 111–113.

Arino, O., M. Simon, I. Piccolini, and J. M. Rosaz (2001), The ERS-2 ATSR-2 world fire atlas and the ERS-2 ATSR-2 world burnt surface projects, paper presented at 8th ISPRS Conference on Physical Measurements and Signatures in Remote Sensing, Aussois, France, 8–12 January.

Artaxo, P., E. T. Fernandes, J. V. Martins, M. A. Yamascoe, P. V. Hobbs, W. Maenhaut, K. M. Longo, and A. Castanho (1998), Large-scale aerosol source apportionment in Amazonia, *J. Geophys. Res.*, *103*, 31,837–31,847.

Brasseur, G. P., J. J. Orlando, and G. S. Tyndall (Eds.) (1999), *Atmospheric Chemistry and Global Change*, pp. 112–114, chap. 13, Oxford Univ. Press, New York.

Cautenet, S., D. Poulet, C. Delon, R. Delmas, J.-M. Grégoire, J. M. Pereira, S. Cherchali, O. Amram, and G. Flouzat (1999), Simulation of carbon monoxide redistribution over central Africa during biomass burning events (Experiment for Regional Sources and Sinks of Oxidants (EXPRESSO)), *J. Geophys. Res.*, *104*, 30,641–30,657.

Chatfield, R. B., J. A. Vastano, L. Li, G. W. Sachse, and V. S. Connors (1998), The Great African plume from biomass burning: Generalizations from a three-dimensional study off TRACE A carbon monoxide, *J. Geophys. Res.*, *103*, 28,059–28,077.

Chin, M., P. Ginoux, S. Kinne, O. Torres, B. N. Holben, B. N. Duncan, R. V. Martin, J. A. Logan, A. Higurashi, and T. Nakajima (2002), Tropospheric aerosol optical thickness from the GOCART model and comparisons with satellite and sun photometer measurements, *J. Atmos. Sci.*, *59*, 461–483.

Chu, D. A., Y. J. Kaufman, C. Ichoku, L. A. Remer, D. Tanré, and B. N. Holben (2002), Validation of MODIS aerosol optical depth retrieval over land, *Geophys. Res. Lett.*, *29*(12), 8007, doi:10.1029/2001GL013205.

Chu, D. A., Y. J. Kaufman, G. Zibordi, J. D. Chern, J. Mao, C. Li, and B. N. Holben (2003), Global monitoring of air pollution over land from the Earth Observing System-Terra Moderate Resolution Imaging Spectroradiometer (MODIS), *J. Geophys. Res.*, *108*(D21), 4661, doi:10.1029/2002JD003179.

Crutzen, P. J., and G. R. Carmichael (1993), Modeling the influence of fires on atmospheric chemistry, in *Fire in the Environment: The Ecological, Atmospheric, and Climate Importance of Vegetation Fires*, edited by P. J. Crutzen and J. G. Goldammer, pp. 89–106, John Wiley, Hoboken, N. J.

Deeter, M. N., et al. (2003), Operational carbon monoxide retrieval algorithm and selected results for the MOPITT instrument, *J. Geophys. Res.*, *108*(D14), 4399, doi:10.1029/2002JD003186.

Deeter, M. N., L. K. Emmons, D. P. Edwards, J. C. Gille, and J. R. Drummond (2004a), Vertical resolution and information content of CO profiles retrieved by MOPITT, *Geophys. Res. Lett.*, *31*, L15112, doi:10.1029/2004GL020235.

Deeter, M. N., et al. (2004b), Evaluation of operational radiances for the Measurements of Pollution in the Troposphere (MOPITT) instrument CO thermal band channels, *J. Geophys. Res.*, *109*, D03308, doi:10.1029/2003JD003970.

de Laat, A. T. J., J. Lelieveld, G. J. Roelofs, R. R. Dickerson, and J. M. Lobert (2001), Source analysis of carbon monoxide pollution during INDOEX 1999, *J. Geophys. Res.*, *106*, 28,481–28,495.

Delmas, R. A., et al. (1999), Experiment for Regional Sources and Sinks of Oxidants (EXPRESSO): An overview, *J. Geophys. Res.*, *104*, 30,609–30,624.

Drummond, J. R. (1992), Measurements of Pollution in the Troposphere (MOPITT), in *The Use of EOS for Studies of Atmospheric Physics*, edited by J. C. Gille and G. Visconti, pp. 77–101, North Holland, New York.

Eck, T. F., B. N. Holben, D. E. Ward, O. Dubovik, A. Smirnov, M. M. Mukelabai, N. C. Hsu, N. T. O'Neil, and I. Slutsker (2001), Characterization of the optical properties of biomass burning aerosols in Zambia during the 1997 ZIBBEE field, campaign, *J. Geophys. Res.*, *106*, 3425–3448.

Eck, T. F., et al. (2003), Variability of biomass burning aerosol optical characteristics in southern Africa during the SAFARI 2000 dry season campaign and a comparison of single scattering albedo estimates from radiometric measurements, *J. Geophys. Res.*, *108*(D13), 8479, doi:10.1029/2002JD002296.

Edwards, D. P., C. Halvorson, and J. C. Gille (1999), Radiative transfer modeling for the EOS Terra Satellite Measurement of Pollution in the Troposphere (MOPITT) instrument, *J. Geophys. Res.*, *104*, 16,755–16,775.

Edwards, D. P., et al. (2003), Tropospheric ozone over the tropical Atlantic: A satellite perspective, *J. Geophys. Res.*, *108*(D8), 4237, doi:10.1029/2002JD002927.

Edwards, D. P., et al. (2004), Observations of carbon monoxide and aerosol from the Terra satellite: Northern Hemisphere variability, *J. Geophys. Res.*, *109*, D24202, doi:10.1029/2004JD004727.

Edwards, D. P., et al. (2006), Southern hemisphere carbon monoxide interannual variability observed by Terra/MOPITT, *J. Geophys. Res.*, doi:10.1029/2005JD007079, in press.

Emmons, L. K., et al. (2004), Validation of Measurements of Pollution in the Troposphere (MOPITT) CO retrievals with aircraft in situ profiles, *J. Geophys. Res.*, *109*, D03309, doi:10.1029/2003JD004101.

Ferek, R. J., J. S. Reid, P. V. Hobbs, D. R. Blake, and C. Liouse (1998), Emission factors of hydrocarbons, halocarbons, trace gases and particles from biomass burning in Brazil, *J. Geophys. Res.*, *103*, 32,107–32,118.

Fishman, J., K. Fakhruzzaman, B. Cros, and D. Nganga (1991), Identification of widespread pollution in the Southern Hemisphere deduced from satellite analyses, *Science*, *252*, 1693–1696.

Fishman, J., V. G. Brackett, E. Browell, and W. B. Grant (1996), Tropospheric ozone derived from TOMS/SBUV measurements during TRACE A, *J. Geophys. Res.*, *101*, 6627–6634.

Fishman, J., A. E. Wozniak, and J. K. Creilson (2003), Global distribution of tropospheric ozone from satellite measurements using the empirically corrected tropospheric ozone residual technique: Identification of the regional aspects of air pollution, *Atmos. Chem. Phys.*, *3*, 893–907.

Formenti, P., W. Elbert, W. Maenhaut, J. Haywood, S. Osborne, and M. O. Andreae (2003), Inorganic and carbonaceous aerosols during the Southern African Regional Science Initiative (SAFARI 2000) experiment: Chemical characteristics, physical properties, and emission data for smoke from African biomass burning, *J. Geophys. Res.*, *108*(D13), 8488, doi:10.1029/2002JD002408.

Galanter, M., H. Levy, and G. R. Carmichael (2000), Impacts of biomass burning on tropospheric CO, NO_x, and O_3, *J. Geophys. Res.*, *105*, 6633–6653.

Garstang, M., P. D. Tyson, R. Swap, M. Edwards, P. Kallberg, and J. A. Lindesay (1996), Horizontal and vertical transport of air over southern Africa, *J. Geophys. Res.*, *101*, 23,721–23,736.

Giglio, L., J. Descloitres, C. O. Justice, and Y. J. Kaufman (2003), An enhanced contextual fire detection algorithm for MODIS, *Remote Sens. Environ.*, *87*, 273–282.

Granier, C., J.-F. Mueller, G. Pétron, and G. Brasseur (1999), A three-dimensional study of the global CO budget, *Chemosphere*, *1*, 255–261.

Gras, J. L., J. B. Jensen, K. Okada, M. Ikegami, Y. Zaizen, and Y. Makino (1999), Some optical properties of smoke aerosol in Indonesia and tropical Australia, *Geophys. Res. Lett.*, *26*, 1393–1396.

Hao, W. M., D. E. Ward, G. Olbu, and S. P. Baker (1996), Emissions of CO_2, CO, and hydrocarbons from fires in diverse African savanna ecosystems, *J. Geophys. Res.*, *101*, 23,577–23,584.

Haywood, J. M., S. R. Osborne, P. N. Francis, A. Keil, P. Formenti, M. O. Andreae, and P. H. Kaye (2003), The mean physical and optical properties of regional haze dominated by biomass burning aerosol measured from the C-130 aircraft during SAFARI 2000, *J. Geophys. Res.*, *108*(D13), 8473, doi:10.1029/2002JD002226.

Hobbs, P. V. (2003), Clean air slots amid dense atmospheric pollution in southern Africa, *J. Geophys. Res.*, *108*(D13), 8490, doi:10.1029/2002JD002156.

Hoell, J. M., D. D. Davis, D. J. Jacob, M. O. Rodgers, R. E. Newell, H. E. Fuelberg, R. J. McNeal, J. L. Raper, and R. J. Bendura (1999), Pacific Exploratory Mission in the tropical Pacific: PEM Tropics A, August–September 1996, *J. Geophys. Res.*, *104*, 5567–5584.

Hoelzemann, J. J., M. G. Schultz, G. P. Brasseur, C. Granier, and M. Simon (2004), Global Wildland Fire Emission Model (GWEM), Evaluating the use of global area burnt satellite data, *J. Geophys. Res.*, *109*, D14S04, doi:10.1029/2003JD003666.

Horowitz, L., et al. (2003), A global simulation of tropospheric ozone and related tracers: Description and evaluation of MOZART, version 2, *J. Geophys. Res.*, *108*(D24), 4784, doi:10.1029/2002JD002853.

Ichoku, C., L. A. Remer, Y. J. Kaufman, R. Levy, D. A. Chu, D. Tanré, and B. N. Holben (2003), MODIS observation of aerosols and estimation of aerosol radiative forcing over southern Africa during SAFARI 2000, *J. Geophys. Res.*, *108*(D13), 8499, doi:10.1029/2002JD002366.

Intergovernmental Panel on Climate Change (2001), *Climate Change 2001*, edited by J. T. Houghton et al., Cambridge Univ. Press, New York.

Jacobson, M. Z. (2001), Strong radiative heating due to the mixing state of black carbon in atmospheric aerosols, *Nature*, *409*, 695–697.

Kanakidou, M., and P. J. Crutzen (1999), The photochemical source of carbon monoxide: Importance, uncertainties and feedbacks, *Chemosphere*, *1*, 91–109.

Kar, J., et al. (2004), Evidence of vertical transport of carbon monoxide from Measurements of Pollution in the Troposphere (MOPITT), *Geophys. Res. Lett.*, *31*, L23105, doi:10.1029/2004GL021128.

Kaufman, Y., D. Tanré, L. Remer, E. Vermote, A. Chu, and B. N. Holben (1997), Remote sensing of tropospheric aerosol from EOS-MODIS over the land using dark targets and dynamic aerosol models, *J. Geophys. Res.*, *102*, 17,051–17,065.

Kaufman, Y., et al. (1998), Smoke, Clouds, and Radiation-Brazil (SCAR-B) experiment, *J. Geophys. Res.*, *103*, 31,783–31,808.

Kaufman, Y., D. Tanré, and O. Boucher (2002a), A satellite view of aerosols in the climate system, *Nature*, *419*, 215–223.

Kaufman, Y., N. Gobron, B. Pinty, J.-L. Widlowski, and M. M. Verstraete (2002b), Relationship between surface reflectance in the visible and mid-IR used in MODIS aerosol algorithm theory, *Geophys. Res. Lett.*, *29*(23), 2116, doi:10.1029/2001GL014492.

Kent, G. S., C. R. Trepte, and P. L. Lucker (1998), Long-term Stratospheric Aerosol and Gas Experiment I and II measurements of upper tropospheric aerosol extinction, *J. Geophys. Res.*, *103*, 28,863–28,874.

Kunhikrishnan, T., M. G. Lawrence, R. von Kuhlmann, A. Richter, A. Ladstatter-Weisenmayer, and J. P. Burrows (2004), Semiannual NO_2 plumes during the monsoon transition periods over the central Indian Ocean, *Geophys. Res. Lett.*, *31*, L08110, doi:10.1029/2003GL019269.

Lacaux, J. P., J. M. Brustet, R. Delmas, J. C. Menaut, L. Abbadie, B. Bonsang, H. Cachier, J. Baudet, M. O. Andreae, and G. Helas (1995), Biomass burning in the tropical savannas of Ivory Coast: An overview of the field experiment Fire Of Savannas (FOS/DECAFE 91), *J. Atmos. Chem.*, *22*, 195–216.

Liu, J., J. R. Drummond, Q. Li, J. C. Gille, and D. C. Ziskin (2005), Satellite mapping of CO emission from forest fires in Northwest America using MOPITT measurements, *Rem. Sens. Environ.*, *95*, 4, 502–516.

Logan, J. A., M. J. Prather, S. C. Wofsy, and M. B. McElroy (1981), Tropospheric chemistry: A global perspective, *J. Geophys. Res.*, *86*, 7210–7254.

Martin, R. V., D. J. Jacob, R. M. Yantosca, M. Chin, and P. Ginoux (2003), Global and regional decreases in tropospheric oxidants from photochemical effects of aerosols, *J. Geophys. Res.*, *108*(D3), 4097, doi:10.1029/2002JD002622.

Pak, B. C., et al. (2003), Measurements of biomass burning influences in the troposphere over southeast Australia during the SAFARI 2000 dry season campaign, *J. Geophys. Res.*, *108*(D13), 8480, doi:10.1029/2002JD002343.

Pétron, G., C. Granier, B. Khattatov, V. Yudin, J. Lamarque, L. Emmons, J. Gille, and D. P. Edwards (2004), Monthly CO surface sources inventory based on the 20,002001 MOPITT satellite data, *Geophys. Res. Lett.*, *31*, L21107, doi:10.1029/2004GL020560.

Pickering, K. E., A. M. Thompson, J. R. Scala, W.-K. Tao, and J. Simpson (1992), Ozone production potential following convective redistribution of biomass burning emissions, *J. Atmos. Chem.*, *14*, 297–313.

Queface, A. J., S. J. Piketh, H. J. Annegarn, B. N. Holben, and R. J. Uthui (2003), Retrieval of aerosol optical thickness and size distribution from the CIMEL Sun photometer over Inhaca Island, Mozambique, *J. Geophys. Res.*, *108*(D13), 8509, doi:10.1029/2002JD002374.

Rasch, P. J., et al. (2000), A comparison of scavenging and deposition processes in global models: Results from the WCRP Cambshop of 1995, *Tellus, Ser. B*, *52*, 1025–1056.

Reid, J. S., P. V. Hobbs, R. J. Ferek, D. R. Blake, J. Vanderlei Martins, M. R. Dunlap, and C. Liousse (1998), Physical, chemical and optical properties of regional hazes dominated by smoke in Brazil, *J. Geophys. Res.*, *103*, 32,059–32,080.

Reid, J. S., T. F. Eck, S. A. Christopher, R. Koppmann, O. Dubovik, D. P. Eleuterio, B. N. Holben, E. A. Reid, and J. Zhang (2005), A review of biomass burning emissions part III: intensive optical properties of biomass burning particles, *Atmos. Chem. Phys.*, *5*, 827–849.

Remer, L. A., et al. (2002), Validation of MODIS aerosol retrieval over ocean, *Geophys. Res. Lett.*, *29*(12), 8008, doi:10.1029/2001GL013204.

Ridley, B. A., S. Madronich, R. B. Chatfield, J. G. Walega, R. E. Shetter, M. A. Carroll, and D. D. Montzka (1992), Measurements and model simulations of the photostationary state during the Mauna Loa Observatory Photochemistry Experiment: Ozone production and loss rates, *J. Geophys. Res.*, *97*, 10,275–10,388.

Rodgers, C. D. (2000), *Inverse Methods for Atmospheric Sounding*, World Sci., Hackensack, N. J.

Schmid, B., et al. (2003), Coordinated airborne, spaceborne, and ground-based measurements of massive, thick aerosol layers during the dry season in southern Africa, *J. Geophys. Res.*, *108*(D13), 8496, doi:10.1029/2002JD002297.

Siegert, F., et al. (2001), Increased damage from fires in logged forests during droughts caused by El Niño, *Nature*, *414*, 437–440.

Silva, J. M. N., J. M. C. Pereira, A. I. Cabral, A. C. L. Sá, M. J. P. Vasconcelos, B. Mota, and J.-M. Grégoire (2003), An estimate of the area burned in southern Africa during the 2000 dry season using SPOT VEGETATION satellite data, *J. Geophys. Res.*, *108*(D13), 8498, doi:10.1029/2002JD002320.

Sinha, P., L. Jaeglé, P. V. Hobbs, and Q. Liang (2004), Transport of biomass burning emissions from southern Africa, *J. Geophys. Res.*, *109*, D20204, doi:10.1029/2004JD005044.

Sobel, A. H., S. E. Yuter, C. S. Bretherton, and G. N. Kiladis (2004), Large-scale meteorology and deep convection during TRMM KWAJEX, *Mon. Weather Rev.*, *132*, 422–444.

Stein, D. C., R. J. Swap, S. Greco, S. J. Piketh, S. A. Macko, B. G. Doddridge, T. Elias, and R. T. Bruintjes (2003), Haze layer characterization and associated meteorological controls along the eastern coastal region of southern Africa, *J. Geophys. Res.*, *108*(D13), 8506, doi:10.1029/2002JD003237.

Swap, R. J., and P. D. Tyson (1999), Stable discontinuities as determinants of the vertical distribution of aerosols and trace gases in the atmosphere, *S. Afr. J. Sci.*, *95*, 63–70.

Swap, R., M. Garstang, S. A. Macko, P. D. Tyson, W. Maenhaut, P. Artaxo, P. Kallberg, and R. Talbot (1996), The long range transport of southern African aerosols to the tropical South Atlantic, *J. Geophys. Res.*, *101*, 23,777–23,791.

Swap, R. J., H. J. Annegarn, J. T. Suttles, M. D. King, S. Platnick, J. L. Privette, and R. J. Scholes (2003), Africa burning: A thematic analysis of the Southern African Regional Science Initiative (SAFARI 2000), *J. Geophys. Res.*, *108*(D13), 8465, doi:10.1029/2003JD003747.

Tanré, D., Y. J. Kaufman, M. Herman, and S. Mattoo (1997), Remote sensing of aerosol over oceans from EOS-MODIS, *J. Geophys. Res.*, *102*, 16,971–16,988.

Tansey, K., et al. (2004), Vegetation burning in the year 2000: Global burned area estimates from SPOT VEGETATION data, *J. Geophys. Res.*, *109*, D14S03, doi:10.1029/2003JD003598.

Thompson, A. M., K. E. Pickering, D. P. McNamara, M. R. Schoeberl, R. D. Hudson, J. H. Kim, E. V. Browell, V. W. J. H. Kirchhoff, and D. Nganga (1996), Where did tropospheric ozone over southern Africa and the tropical Atlantic come from in October 1992?: Insights from TOMS, GTE TRACE A, and SAFARI 1992, *J. Geophys. Res.*, *101*, 24,251–24,27.

Thompson, A. M., et al. (2003), Southern Hemisphere Additional Ozonesonde (SHADOZ) 1998 2000 tropical ozone climatology: 2. Tropospheric variability and the zonal wave-one, *J. Geophys. Res.*, *108*(D2), 8241, doi:10.1029/2002JD002241.

Tie, X., S. Madronich, S. Walters, D. P. Edwards, P. Ginoux, N. Mahowald, R. Zhang, C. Lou, and G. Brasseur (2005), Assessment of the global impact of aerosols on tropospheric oxidants, *J. Geophys. Res.*, *110*, D03204, doi:10.1029/2004JD005359.

Valks, P. J. M., R. B. A. Koelemeijer, M. van Weele, P. van Velthoven, J. P. F. Fortuin, and H. Kelder (2003), Variability in tropical tropospheric ozone: Analysis with Global Ozone Monitoring Experiment observations and a global model, *J. Geophys. Res.*, *108*(D11), 4328, doi:10.1029/2002JD002894.

van der Werf, G. R., J. T. Randerson, G. J. Collatz, and L. Giglio (2003), Carbon emissions from fires in tropical and subtropical ecosystems, *Global Change Biol.*, *9*, 547–562.

Ward, D. E., W. M. Hao, R. A. Susott, R. E. Babbitt, R. W. Shea, J. B. Kauffman, and C. O. Justice (1996), Effect of fuel composition on combustion efficiency and emission factors for African savanna ecosystems, *J. Geophys. Res.*, *101*, 23,569–23,576.

Wolter, K., and M. S. Timlin (1998), Measuring the strength of ENSO: How does 1997/98 rank?, *Weather*, *53*, 315–324.

J.-L. Attié, Laboratoire d'Aérologie, Observatoire Midi-Pyrénées, 14 Av. E. Belin, F-31400 Toulouse, France. (attjl@aero.obs-mip.fr)

A. Chu, Joint Center for Earth Systems Technology, University of Maryland, Baltimore County, 1000 Hilltop Circle, Baltimore, MD 21250, USA. (achu@climate.gsfc.nasa.gov)

M. N. Deeter, D. P. Edwards, L. K. Emmons, J. C. Gille, S. T. Massie, and D. C. Ziskin, National Center for Atmospheric Research, P.O. Box 3000, Boulder, CO 80307-3000, USA. (mnd@ucar.edu; edwards@ucar.edu; emmons@ucar.edu; gille@ucar.edu; massie@ucar.edu; ziskin@ucar.edu)

J. R. Drummond, Department of Physics, University of Toronto, St George Street, Toronto, Ontario, M5S 1AS, Canada. (james.drummond@utoronto.ca)

L. Giglio, NASA Goddard Space Flight Center, Greenbelt, MD 20771, USA. (giglio@hades.gsfc.nasa.gov)

J. Haywood, Met Office, Exeter, Devon, EX1 3PB, UK. (jim.haywood@metoffice.gov.uk)

S. W. Wood, National Institute of Water and Atmospheric Research Ltd, Lauder, Private Bag 50061, Omakau, Central Otago, New Zealand. (s.wood@niwa.co.nz)